Evolution of coherent collective modes through consecutive charge-density-wave transitions in the $(PO_2)_4(WO_3)_{12}$ monophosphate tungsten bronze

L. Stojchevska,[1] M. Borovšak,[1,2] P. Foury-Leylekian,[3] J.-P. Pouget,[3] T. Mertelj,[1,4,*] and D. Mihailovic[1,2,4]

[1]*Complex Matter Department, Jozef Stefan Institute, Jamova 39, 1000 Ljubljana, Slovenia*

[2]*Faculty of Mathematics and Physics, University of Ljubljana, Jadranska 19, 1000 Ljubljana, Slovenia*

[3]*Laboratoire de Physique des Solides, UMR CNRS 8502, Université Paris Sud, 91405 Orsay - France*

[4]*Center of Excellence on Nanoscience and Nanotechnology Nanocenter (CENN Nanocenter), Jamova 39, 1000 Ljubljana, Slovenia*

All-optical femtosecond relaxation dynamics in a single crystal of monophosphate tungsten bronze $(PO_2)_4(WO_3)_{2m}$ with alternate stacking $m = 6$ of WO_3 layers was studied through the three consequent charge-density-wave (CDW) transitions. Several transient coherent collective modes associated with the different CDW transitions were observed and analyzed in the framework of the time-dependent Ginzburg–Landau theory. Remarkably, the interference of the modes leads to an *apparent rectification* effect in the transient reflectivity response. A saturation of the coherent-mode amplitudes with increasing pump fluence well below the CDWs destruction threshold fluence indicates a decoupling of the electronic and lattice parts of the order parameter on the femtosecond timescale.

I. INTRODUCTION

Time-resolved spectroscopy can give unique insight into the dynamical behavior of the elementary excitations in systems undergoing charge-density-wave (CDW) transitions. The appearance of new collective vibrational excitations in Raman [1–3] and coherent transient reflectivity [4–6] response upon charge-density-wave formation is well documented [1–7] and theoretically quite well understood [7]. In systems with more than one CDW transition new collective modes are expected to appear below each transition temperature, as observed experimentally in the Raman response [2,3]. In the transient reflectivity response [6,8], however, the additional coherent oscillation modes below the subsequent CDW transition temperatures have not been readily observed. Investigating the differences in the response associated with different transitions gives important information on the coupling and damping of collective modes, and behavior of the order parameter in each case.

The monophosphate tungsten bronzes $(PO_2)_4(WO_3)_{2m}$ are an example of low-dimensional CDW materials [9] offering a possibility to further explore the effect of consecutive CDW transitions on the transient-reflectivity coherent oscillatory response. They are quasi-two-dimensional (2D) conductors built from layers of WO_6 octahedra parallel to the (a,b) plane and separated by PO_4 tetrahedra [10–13] as shown in Fig. 1. Their electronic properties arise from quasi-one-dimensional chain structures where—due to the strong Fermi surface nesting—charge-density-wave (CDW) instabilities develop below certain critical transition temperatures T_{CDW}, as confirmed by various experimental techniques [10,14,15]. For $(PO_2)_4(WO_3)_{2m}$ with $m = 6$ in particular three CDW transitions have been observed: $T_{CDW1} = 120$ K, $T_{CDW2} = 62$ K, and $T_{CDW3} = 30$ K [9,10,16].

To date, a substantial effort has been put into studying the electronic, magnetic, and structural properties of $(PO_2)_4(WO_3)_{2m}$ bronzes [17–19]; however, to the best of our knowledge there is no Raman or time-resolved optical spectroscopy study of the sequence of CDW phases in $(PO_2)_4(WO_3)_{2m}$ tungsten bronzes. In this paper we therefore report on temperature and fluence dependence of the transient reflectivity in a monophosphate tungsten bronze $(PO_2)_4(WO_3)_{2m}$ single crystal with $m = 6$ ($P_4W_{12}O_{44}$) on a femtosecond timescale, focusing on the effect of the subsequent CDW transitions on the coherent oscillatory transient response.

II. EXPERIMENT

Single crystals used in this study were grown at CRISMAT (Caen, France) according to a previously reported method [20]. They have a shape of platelets with large surface of about (1×1.5) mm^2, corresponding to the (a,b) conducting plane, and a thickness of $\sim 1/10$ mm along c. The index $m = 6$ of the bronze was unambiguously determined by the measurement of the interslab periodicity [11] c ($c = 23.57$ for $m = 6$).

Optical experiments were performed with 50 fs laser pulses at 800 nm generated from an amplified Ti:sapphire mode-locked laser at a 250 kHz repetition rate. The transient reflectivity $\Delta R/R = \frac{R_p - R_0}{R_0}$, where R_p and R_0 are the reflectivities in the presence and absence of the pump pulse, respectively, was monitored by using a standard pump-probe technique where both pump and probe photons were at 1.55 eV photon energy. The beam diameters on the sample were determined by means of calibrated pinholes to be 108 μm and 50 μm for the pump and probe beam, respectively. Both beams were perpendicularly polarized to each other and oriented relatively to the crystal axes in a way to obtain maximum or minimum response amplitude at low temperatures. Before optical measurements the single crystals were cleaved by means of scotch tape and mounted on a cold finger of a liquid-He flow optical cryostat equipped with CaF$_2$ windows.
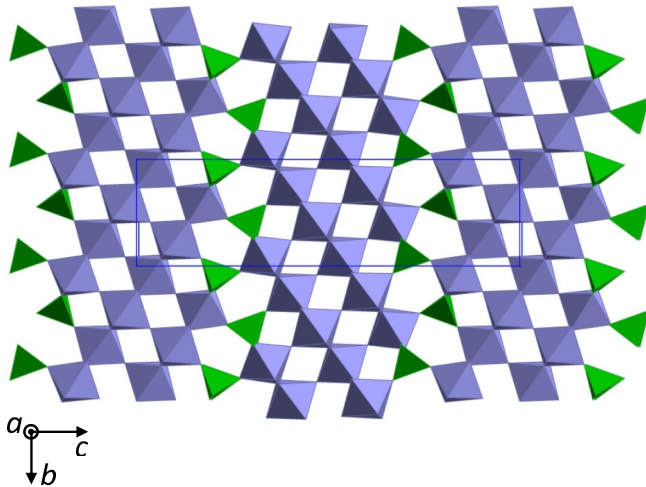
*tomaz.mertelj@ijs.si

FIG. 1. Crystal structure of $(PO_2)_4(WO_3)_{12}$ showing the WO_6 octahedra and the monophosphate PO_4 tetrahedra projected along the a crystallographic direction.

III. RESULTS

A. Experimental data

In Fig. 2 we show the temperature dependence of the transient reflectivity ($\Delta R/R$) in $(PO_2)_4(WO_3)_{12}$ taken at a pump fluence of 8 μJ/cm^2. The response is characterized by four main features:

(1) A subpicosecond negative transient (feature A), which changes only little with decreasing T.

(2) A prominent picosecond negative transient (feature B) that appears on top of feature A below $T_{CDW2} = 62$ K. Remarkably, feature B (Fig. 2) *displays a risetime that appears slightly longer than the decay time*.

(3) A small positive feature C (see Fig. 2) peaked at $\sim$0.5 ps that appears below $T_{CDW1} = 120$ K and develops into a weak oscillation when approaching T_{CDW2}.

(4) A negative shoulder together with additional weak oscillations beyond $\sim$2 ps delay (feature D in Fig. 2), that appear below the lowest transition at $T_{CDW3} = 30$ K.

The feature-D weak oscillations were not completely reproducible between different experimental runs. While the T dependence shown in Fig. 2(c) was measured in the first run immediately after cleaving the sample the data shown in Fig. 2(b) were measured in the second run after keeping the sample in vacuum for 12 days. Since it is not possible to measure exactly the same sample spot in different runs it is not clear whether the difference can be attributed to deterioration of the sample surface or surface inhomogeneity.

In Fig. 3 we plot the pump fluence dependence of the transient reflectivity measured at $T = 5$ K during the first run. The magnitude of the transients shows saturation with increasing $\mathcal{F}$ above $\sim$20 μJ/cm^2. With further fluence increase the response changes qualitatively above $\mathcal{F} \simeq 80$ μJ/cm^2 as shown in the inset of Fig. 3.

B. Analysis

An unusual feature of the data, which we need to understand, is that at the lowest temperatures the risetime of feature
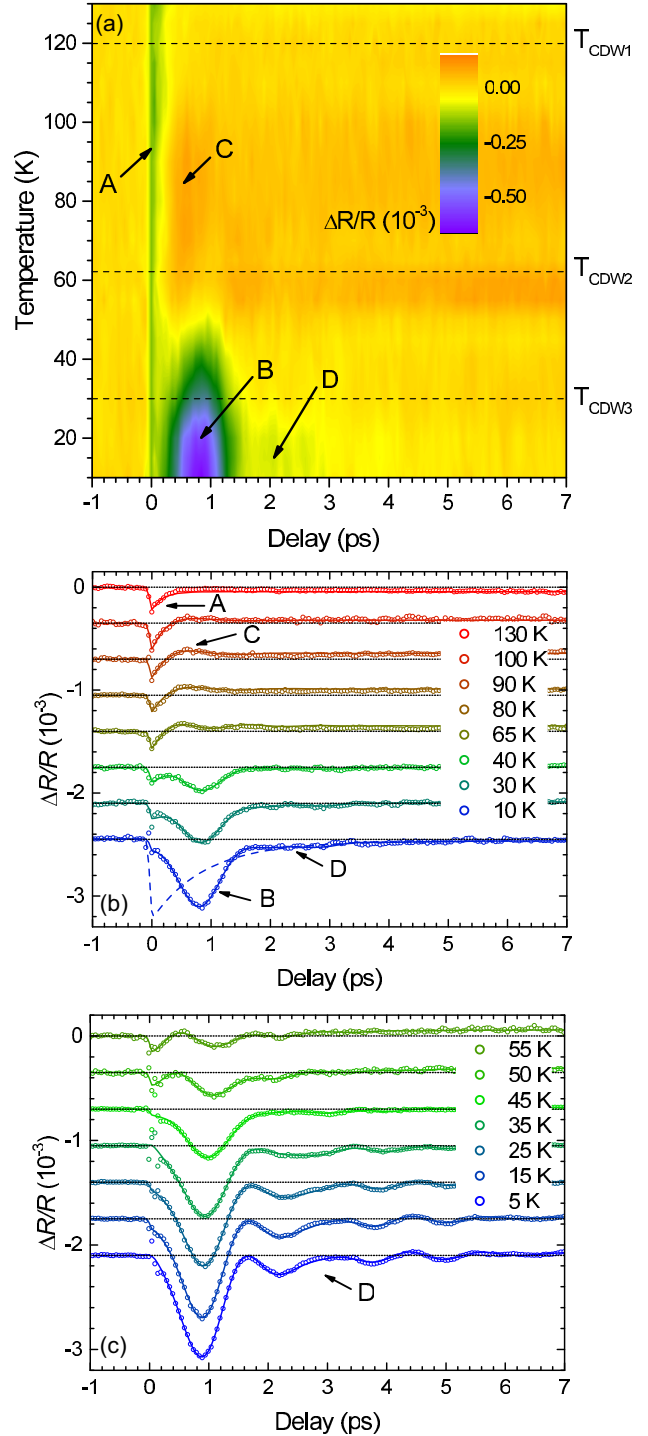

FIG. 2. (a) Temperature dependence of the transient reflectivity in $(PO_2)_4(WO_3)_{12}$ measured at the 8 μJ/cm^2 pump fluence. Horizontal dashed lines in panel (a) indicate the transition temperatures: $T_{CDW1} = 120$ K, $T_{CDW2} = 62$ K, and $T_{CDW3} = 30$ K. (b), (c) The transient reflectivity at selected temperatures together with the DCE-model fits (continuous lines). Panels (b) and (c) correspond to different experimental runs (see text) where panel (c) is focused on the CDW3-transition T region with a finer T step. The transients are vertically shifted for clarity with the dotted lines indicating the shifts. The dashed line in panel (b) corresponds to the the displaced equilibrium position for oscillators at 10 K. There is a notable coherent artifact due to the pump scattering appearing as increased noise at zero delay.
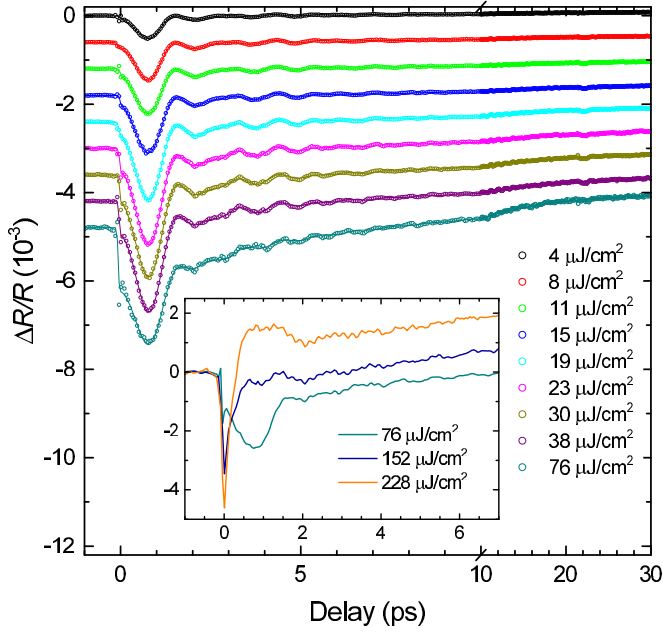
FIG. 3. Pump-fluence dependence of the transient reflectivity at 5 K. The traces are vertically shifted for clarity. The thin lines are the DCE-model fits discussed in text. The inset shows the qualitative change at the fluences above 76 μJ/cm^2.

B apparently exceeds the decay time. Due to the ubiquitous appearance of a coherent collective oscillations in the transient reflectivity upon CDW formation [4–6] it is very likely that the unusual shape of feature B is due to an interference between coherent oscillations. To test this hypothesis and get better insight into the unusual shape of feature B we fit the data using the theory of displacive coherent excitation (DCE) of oscillatory modes [21]:

$$\frac{\Delta R}{R} = \left(A_{\mathrm{displ}} - \sum A_{\mathrm{O}i} \right) \int_0^\infty G(t-u) e^{-u/\tau_{\mathrm{displ}}} du$$

$$+ \sum A_{\mathrm{O}i} \int_0^\infty G(t-u) e^{-\gamma_i u} [\cos(\Omega_i u)$$

$$- \beta_i \sin(\Omega_i u)] du$$

$$+ \sum_{j \in \{1,2\}} A_{\mathrm{e}j} \int_0^\infty G(t-u) e^{-u/\tau_j} du, \qquad (1)$$

with $\beta_i = (1/\tau_{\mathrm{displ}} - \gamma_i)/\Omega_i$ and $G(t) = \sqrt{2/\pi} \tau_{\mathrm{p}}^{-1} \exp(-2t^2/\tau_{\mathrm{p}}^2)$. τ_{p} is the effective pump-probe pulse cross-correlation width, $A_{\mathrm{O}i}$, Ω_i, γ_i are oscillator amplitudes, frequencies, and damping factors, respectively, while $A_{\mathrm{e}j}$ and τ_j are amplitudes and relaxation times of the overdamped exponentially relaxing modes.

We also assume that all oscillators are driven by a single-exponential term with the relaxation time τ_{displ}, while the remaining exponential relaxations are kept independent from the oscillators. Note that the oscillator coordinates contain both the exponentially relaxing and oscillatory components.

As shown in Fig. 4 it is possible to fit[1] the main features of the data using four oscillators at ~1, ~0.8, ~0.7, and

---

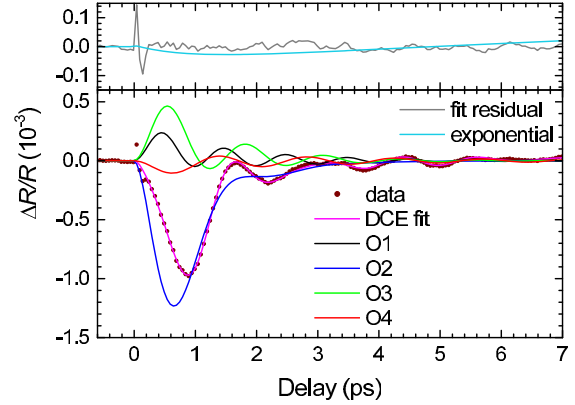[1]Please see also Appendix.

FIG. 4. Components of the DCE-model fit at $T = 5$ K. The destructive interference of O2 with O1 and O3 results in the slow leading edge of feature B.

~0.6 THz with two independent exponential relaxations ($\tau_1 \sim 20$ ps and $\tau_2 \sim 10$ ns) in addition to the main relaxation component ($\tau_{\mathrm{displ}} \lesssim 1$ ps) that drives the oscillators. Fourier transforms of the fit residua (see Appendix) reveal additional four clearly resolvable modes at the lowest T.

IV. DISCUSSION

The presence of collective coherent oscillatory excitations in the photoinduced transient response of various CDWs is ubiquitous [4–6,23–25] and comes from the coupling of phonons to the electronic order parameter which drives the transition [7]. In most cases several weakly damped coherent oscillations are observed well below the CDW transition temperatures, with widely different degrees of softening when approaching the transition from below [4–6,25,26]. The softening has been parametrized using the time-dependent Ginzburg–Landau (TDGL) theory [7,22] by the adiabaticity ratio:

$$a = \kappa m^2 / \Omega_0^3, \qquad (2)$$

where κ is the bare damping of the electronic mode, Ω_0 is the bare phonon frequency, and m is the coupling between the electronic order parameter and the bare phonon mode. $a \gg 1$ corresponds to the adiabatic limit corresponding to the strongest degree of phonon softening. $a \sim 1$ corresponds to the nonadiabatic case with no softening and increased damping of the oscillatory component when approaching the transition temperature from below. In this case the soft mode is the critically damped solution dominated by the electronic order parameter [22].

In the case of $(\mathrm{PO}_2)_4(\mathrm{WO}_3)_{12}$ the main coherent oscillations at ~1 and ~0.6 THz appear strongly damped down to the lowest T with significantly weaker less-damped modes observed only below T_{CDW3}.

Despite being rather weak the 1 THz mode (O1) could be associated with the formation of CDW1 at T_{CDW1}. When approaching T_{CDW1} from below (see Fig. 5) it softens by ~50% and with an increase of damping vanishes above ~100 K.
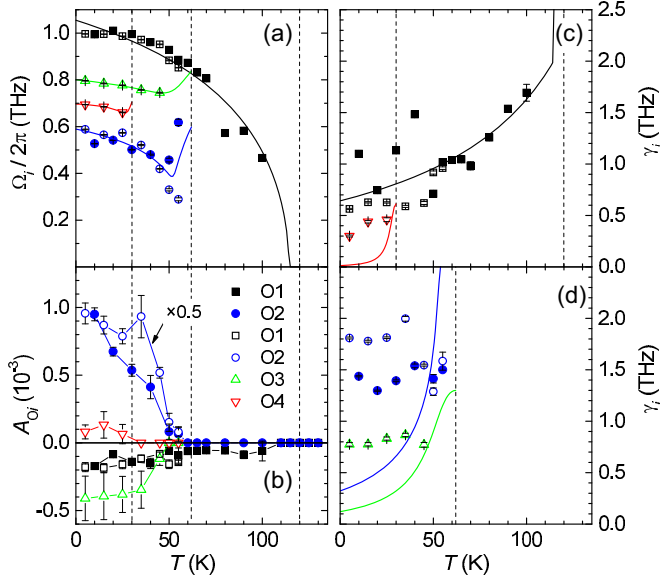
FIG. 5. Temperature dependence of the oscillatory-modes DCE-model fit parameters. The continuous lines in panels (a), (c), and (d) are the TDGL theory [7,22] fits. Full and open symbols represent data from two separate experimental runs from Fig. 2. The vertical dashed lines correspond to the three CDW transition temperatures.
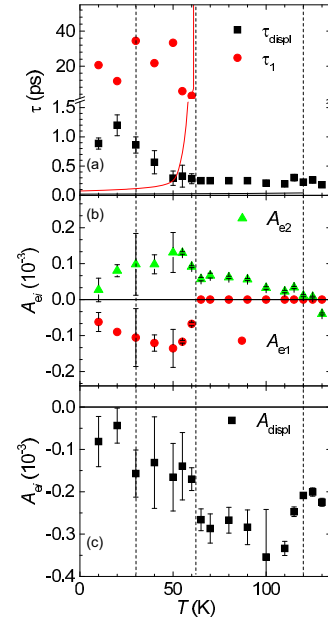

FIG. 6. Temperature dependence of the exponential-modes DCE-model fit parameters from Fig. 2. The red continuous line in panel (a) is the TDGL theory [7,22] prediction corresponding to the mode-O2 fit in Fig. 5. The vertical dashed lines correspond to the three CDW transition temperatures.

Below T_{CDW2} two additional modes appear. The strongest is the ~ 0.5 THz mode (O2) which shows $\sim 30\%$ softening with increasing T and vanishes above 55 K. Above 50 K the frequency shows large scatter between the two experimental runs, presumably due to a small amplitude and rather large damping that couples the fit parameters of modes O1 and O2. The second mode at ~ 0.8 THz (O3) is weaker, but less damped with a softening of less than 10% disappearing above $T \sim 50$ K.

Below T_{CDW3} another two modes appear. The strongest ~ 0.7 THz mode (O4) shows $\sim 5\%$ softening with increasing T, while the weaker one at ~ 1.2 THz, that was not included in the fits (see Appendix) shows virtually no softening.

The other three higher-frequency modes, which were observed in fit residuals at higher fluences (see Appendix) cannot be clearly associated with any of the transitions due to the weak intensities at the pump fluence used for the T scans.

The T dependence of the mode frequencies is consistent with predictions of the TDGL model [7,22] as shown in Fig. 5(a). However, except for mode O1 [see Figs. 5(c) and 5(d)] it is not possible to obtain simultaneous good fits for damping. The experimental dampings greatly exceed the model predictions for modes O2, O3, and O4, except near the CDW transitions, where the model dampings increase.

TABLE I. The main TDGL-theory parameters for oscillatory modes.

Mode	$\Omega_{expt}/2\pi$ (THz)	$\Omega_0/2\pi$ (THz)	a	T_{CDW} (K)
O1	1.0	1.6	2.8	120
O2	0.53	0.75	1.2	62
O3	0.79	0.79	0.3	62
O4	0.69	0.71	0.3	30

We attribute excess damping at lower T to the combination of extrinsic and intrinsic phonon damping that is not directly related to the CDWs and is not included in the TDGL model [7,22]. The model also predicts a region of critical damping for mode O1 just below T_{CDW1} which is due to the vanishing amplitude experimentally inaccessible.

The main TDGL-theory parameters are shown in Table I. The bare frequencies of modes O1 and O2 appear strongly renormalized by the coupling to the electronic order parameter, while the renormalization is small for the other modes.

The model [7] also predicts a second critically damped mode, that is weakly T dependent in the adiabatic case and softens at T_{CDW} in the nonadiabatic case. For CDW1 the mode-O1 fit in Figs. 5(a) and 5(c) implies a fast virtually T-independent mode with $\tau \sim 20$–50 fs, which is ten times faster that the fastest observed relaxation. If the excitation goes through a displacive mechanism involving electrons in the ungapped bands the fast mode would adiabatically follow the displacive drive, resulting in the response consistent with the data.

In contrast, for CDW2 and CDW3 the fits to modes O2, O3, and O4 in Fig. 5(a) imply overdamped soft modes with rather fast relaxation times diverging at the corresponding T_{CDW} as shown for mode O2 by the red solid line in Fig. 6(a). None of the three observed exponential relaxation components (τ_{displ}, τ_1, and τ_2) show such a divergence and therefore cannot be directly associated with the overdamped part of the order-parameter dynamics. This indicates that photons at the energy used in the present experiment (1.55 eV) are only weakly coupled to the electronic order parameters associated with CDW2 and CDW3.
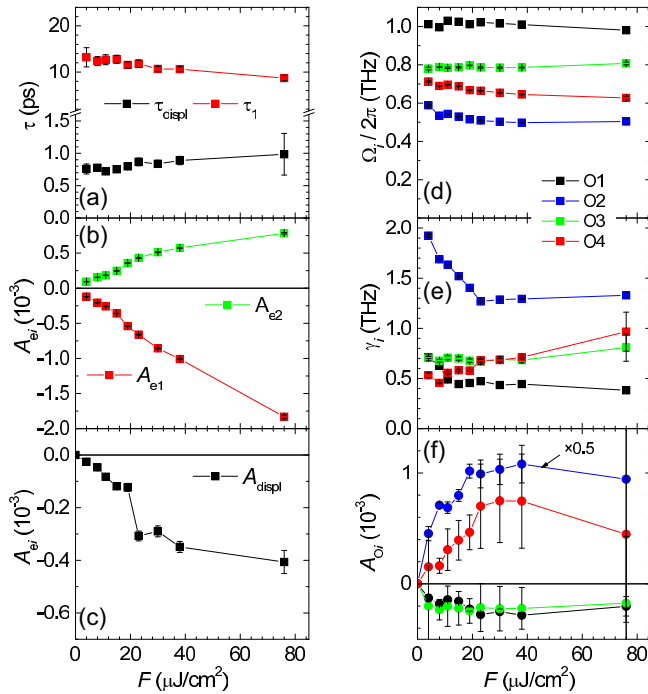
FIG. 7. Fluence dependence of the DCE-model fit parameters at $T = 5$ K from Fig. 3.

The present behavior is different from observations [8] in structurally similar[2] η-Mo$_4$O$_{11}$ where a diverging relaxation time of the overdamped soft mode is clearly observed while the phonon modes associated with the CDW formation show virtually no softening when approaching the CDW transition temperature. This is consistent with the the nonadiabatic limit of the TDGL theory. One of the reasons for a smaller adiabaticity ratio a [see Eq. (2)] could be higher frequencies of the CDW related modes (1.93, 2.19 and 2.94 THz) in η-Mo$_4$O$_{11}$ originating in the smaller Mo mass.

Looking at the pump fluence dependence of the DCE-model fit parameters in Fig. 7 we observe a clear saturation of the coherent-oscillatory-mode amplitudes above $\mathcal{F}_{sat} \sim 20 \ \mu$J/cm^2 while the amplitudes of the exponential relaxation components show only a slightly sublinear behavior. Surprisingly, within error bars the amplitudes of all the oscillatory modes[3] saturate at the same fluence. Except for the damping of the strongest mode O2 the other coherent-oscillatory-mode parameters also show no strong changes around $\mathcal{F}_{sat}$ and remain nearly constant up to $\mathcal{F} \sim 80 \ \mu$J/cm^2.

Previously it has been shown that increasing the pump fluence transiently suppresses and eventually destroys the CDW order [23–25,27]. Since in our experiment the CDW-induced modes remain clearly visible up to $\mathcal{F} \sim 80 \ \mu$J/cm^2 and are completely suppressed only at higher fluences the saturation

at $\mathcal{F}_{sat}$ cannot be attributed to the complete destruction of CDWs. It is, however, unusual that even the amplitude of mode O4 associated with the weakest CDW3 shows only a moderate additional suppression with increasing $\mathcal{F}$ above $\mathcal{F}_{sat}$.

A similar behavior in $1T$-TiSe$_2$, where the periodic lattice distortion (PLD) persists upon destruction of the electronic ordering, has been attributed [28] to sequential suppression of the electronic excitonic component of the CDW order at a lower pump fluence and the Jahn–Teller component at a higher pump fluence. In the case of $(PO_2)_4(WO_3)_{12}$ it is believed that the CDWs are well described in the framework of the Peierls-like mechanism with "hidden" nesting vectors [9,10]. In this picture the PLD and the electronic part of the order parameter work in conjunction to form CDWs. However, *on a short timescale they can become decoupled* due to their different intrinsic timescales. The saturation of the coherent-oscillatory-mode amplitudes can be therefore attributed to such decoupling. In the case when the electronic parts of CDWs are transiently completely suppressed and partially recover on a timescale $\tau_{rec} \ll \Omega_i^{-1}$ the PLDs cannot be completely suppressed. The rather short relaxation times, $\tau_i \lesssim 100$ fs, of the overdamped modes suggested by the TDGL model fits are consistent with such a scenario.

Independently of the above saturation scenario, the decrease of the mode O2 damping with increasing fluence below $\mathcal{F}_{sat}$ could be attributed to the inhomogeneous excitation profile. Due to the finite light penetration depth the CDWs are more strongly suppressed near the surface. The relative contribution of the near-surface part of the excited volume to the response is therefore decreased leading to a decrease of damping in the case of an enhanced extrinsic damping of the mode due the surface effects.

V. SUMMARY AND CONCLUSIONS

We investigated the effect of a sequence of three consecutive CDW transitions in a monophosphate tungsten bronze $(PO_2)_4(WO_3)_{2m}$ ($m = 6$) on the photoinduced ultrafast transient coherent oscillatory optical response. We clearly observe the appearance of new coherent oscillatory modes below each CDW transition. At low T the interference of two rather strongly damped modes at ~ 1 and ~ 0.5 THz, which can be associated with CDW1 at 120 K and CDW2 at 62 K, respectively, leads to an unusual *rectified* transient reflectivity with an inverted-Gaussian shape.

The T dependence of the coherent mode frequencies can be well described within the framework of the recently proposed TDGL model [7,22]. The damping of the most strongly coupled mode at ~ 1 THz, which is coupled with CDW1 order parameter, is consistent with the TDGL model. On the other hand, the less strongly coupled modes associated with CDW2 and CDW3 show an additional intrinsic damping that does not originate from the coupling to the electronic order parameters.

Contrary to the oscillatory modes, no corresponding overdamped modes predicted by the TDGL model are observed by using probe photons at 1.5 eV, which may be explained to be due to weak coupling between the 1.55 eV photons and the electronic parts of the respective order parameters.

---

[2]Both compounds contain similar octahedral layers separated by tetrahedral units, but with different stacking.

[3]The amplitude of mode O3 appears saturated below the lowest measured pump fluence. We believe that this is a fit artifact due to a strong correlation of the fit amplitude with mode O4, which has a very similar frequency, but the opposite phase.
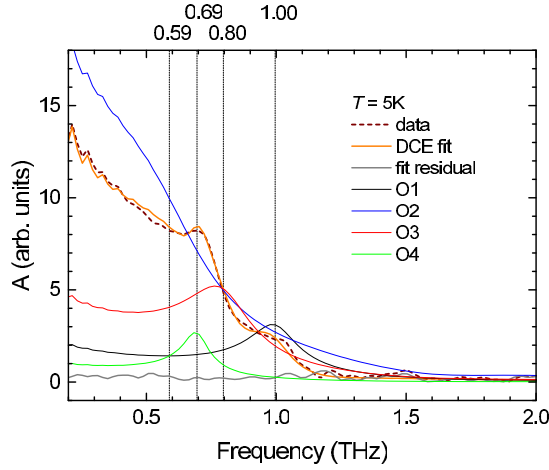
FIG. 8. The Fourier transform spectrum of the data at $T = 5$ K compared with the Fourier transform spectra of the DCE fit, the fit residual, and the individual oscillators. The frequencies of the oscillators obtained from the DCE fit are indicated by vertical lines. Please note that the Fourier transform amplitude of complex spectra are shown so *seemingly* individual components do not add up properly.

Further broadband-probe transient reflectivity studies would be necessary to possibly reveal the overdamped modes.

Upon increasing the pump fluence we observe a saturation of the coherent mode amplitudes well below the complete destruction of the CDWs. This could be attributed to a decoupling of the electronic and lattice parts of the order parameter resulting in a complete ultrafast transient suppression and a partial recovery of the electronic part of the order parameter on a timescale much shorter than the coherent-mode periods.
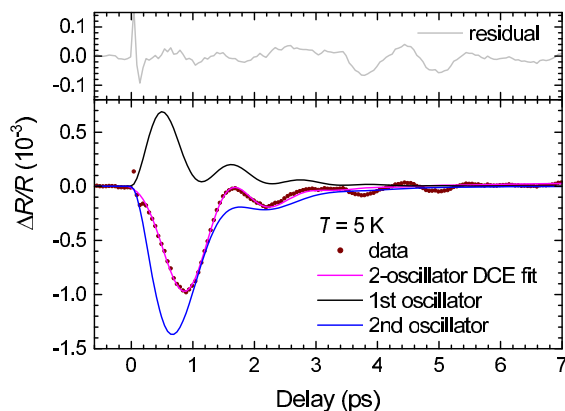
FIG. 9. While a two oscillator-only DCE model reproduces feature B rather well it does not fit the low-T data at longer delays (feature D).
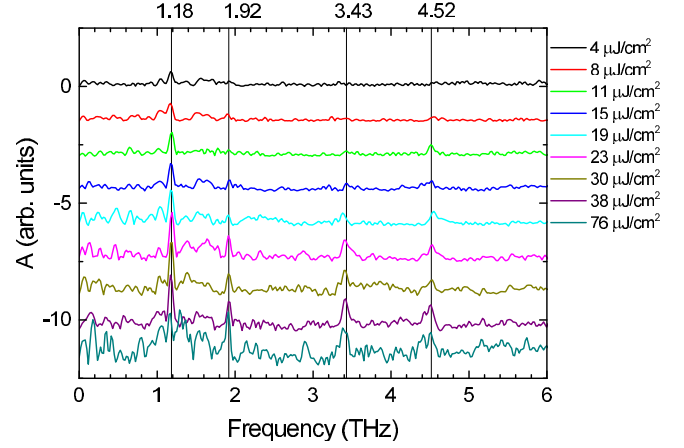

FIG. 10. Fluence dependence of the Fourier transform spectra of the four-oscillator DCE-model fit residuals at $T = 5$ K (see Fig. 3 for the data and fits). The model completely fits the response below 1 THz. The traces are vertically shifted and the main remaining coherent oscillation peaks are indicated by vertical lines.

APPENDIX

Decomposition of Transient Reflectivity into Components

Due to the displacive excitation the strongly damped oscillators show significant spectral density down to zero frequency and are not well resolved in Fourier transform spectra of data, as shown in Fig. 8. Moreover, due to the fixed relative phase overlapping modes often show a Fano-like shape with an absence of a peak at the center frequency (see
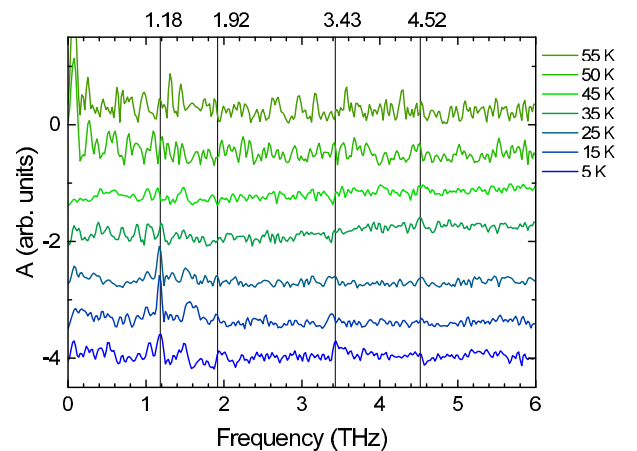

FIG. 11. Fourier transform spectra of the the four-oscillator DCE-model fit residuals in the low-T region [see Fig. 2(c) for the data and fits]. The traces are vertically shifted and the positions of the main remaining coherent oscillation peaks obtained from Fig. 10 are indicated by vertical lines.

mode O3 in Fig. 8). To resolve individual components a real time analysis using DCE-model (1) is therefore necessary.

While a two-oscillator DCE model can fit the initial unusual feature B rather well (see Fig. 9), it fails to fit the oscillations beyond ∼3 ps. Two additional oscillators are needed to reasonably fit the oscillations that appear beyond ∼3 ps at low T.

Further analysis of the four-oscillator DCE-fit residuals at higher fluences (see Fig. 10) reveals at least four additional clearly resolvable modes above 1 THz. The 1.18-THz mode vanishes above $T = 35$ K (Fig. 11) while the T dependence of the other modes cannot be clearly resolved due to their weak intensities.

[1] G. Travaglini, I. Mörke, and P. Wachter, Solid State Commun. **45**, 289 (1983).

[2] S. Sugai, Phys. Status Solidi B **129**, 13 (1985).

[3] M. Lavagnini, H.-M. Eiter, L. Tassini, B. Muschler, R. Hackl, R. Monnier, J.-H. Chu, I. R. Fisher, and L. Degiorgi, Phys. Rev. B **81**, 081101 (2010).

[4] J. Demsar, K. Biljaković, and D. Mihailovic, Phys. Rev. Lett. **83**, 800 (1999).

[5] K. Shimatake, Y. Toda, and S. Tanda, Phys. Rev. B **75**, 115120 (2007).

[6] R. V. Yusupov, T. Mertelj, J. H. Chu, I. R. Fisher, and D. Mihailovic, Phys. Rev. Lett. **101**, 246402 (2008).

[7] H. Schäfer, V. V. Kabanov, M. Beyer, K. Biljakovic, and J. Demsar, Phys. Rev. Lett. **105**, 066402 (2010).

[8] M. Borovšak, L. Stojchevska, P. Sutar, T. Mertelj, and D. Mihailovic, Phys. Rev. B **93**, 125123 (2016).

[9] P. Foury, J. P. Pouget, E. Wang, and M. Greenblatt, Europhys. Lett. **16**, 485 (1991).

[10] P. Foury and J. P. Pouget, Int. J. Mod. Phys. B **07**, 3973 (1993).

[11] P. Roussel, O. Perez, and P. Labbe, Acta Crystallogr., Sect. B: Struct. Sci. **57**, 603 (2001).

[12] P. Foury and J. P. Pouget, Solid State Sci. **4**, 387 (2002).

[13] V. V. Skopenko, V. V. Lisnyak, N. V. Stus, and N. S. Slobodyanik, Russ. Chem. Rev. **73**, 753 (2004).

[14] C. Schlenker, C. Hess, C. Le Touze, and J. Dumas, J. Phys. I France **6**, 2061 (1996).

[15] M. Greenblatt, *Physics and Chemistry of Low-Dimensional Inorganic Conductors* (Plenum Press, New York, 1996), Chap. 2, p. 15.

[16] E. Wang, M. Greenblatt, Idris El-Idrissi Rachidi, E. Canadell, M. H. Whangbo, and S. Vadlamannti, Phys. Rev. B **39**, 12969 (1989).

[17] C. Schlenker, *Low-Dimensional Electronic Properties of Molybdenum Bronzes and Oxides* (Kluwer Academic Press, Dordrecht, 1989).

[18] M. Greenblatt, Int. J. Mod. Phys. B **07**, 3937 (1993).

[19] C. Schlenker, *Physics and Chemistry of Low-Dimensional Inorganic Conductors* (Plenum Press, New York, 1996), Chap. 8, p. 115.

[20] Ph. Labbé, M. Goreaud, and B. Raveau, J. Solid State Chem. **61**, 324 (1986).

[21] H. J. Zeiger, J. Vidal, T. K. Cheng, E. P. Ippen, G. Dresselhaus, and M. S. Dresselhaus, Phys. Rev. B **45**, 768 (1992).

[22] H. Schaefer, V. V. Kabanov, and J. Demsar, Phys. Rev. B **89**, 045106 (2014).

[23] F. Schmitt, P. S. Kirchmann, U. Bovensiepen, R. G. Moore, L. Rettig, M. Krenz, J.-H. Chu, N. Ru, L. Perfetti, D. H. Lu, M. Wolf, I. R. Fisher, and Z.-X. Shen, Science **321**, 1649 (2008).

[24] L. Perfetti, P. A. Loukakos, M. Lisowski, U. Bovensiepen, M. Wolf, H. Berger, S. Biermann, and A. Georges, New J. Phys. **10**, 053019 (2008).

[25] A. Tomeljak, H. Schäfer, D. Städter, M. Beyer, K. Biljakovic, and J. Demsar, Phys. Rev. Lett. **102**, 066404 (2009).

[26] J. Demsar, L. Forro, H. Berger, and D. Mihailovic, Phys. Rev. B **66**, 041101 (2002).

[27] R. Yusupov, T. Mertelj, V. V. Kabanov, S. Brazovskii, P. Kusar, J.-H. C. Chu, I. R. Fisher, and D. Mihailovic, Nat. Phys. **6**, 681 (2010).

[28] M. Porer, U. Leierseder, J.-M. Ménard, H. Dachraoui, L. Mouchliadis, I. Perakis, U. Heinzmann, J. Demsar, K. Rossnagel, and R. Huber, Nat. Mater. **13**, 857 (2014).